# Dual Melting Endotherms in the Thermal Analysis of Poly(ethylene terephthalate)

GAO QIU,[1] ZHI-LIAN TANG,[1] NAN-XUN HUANG,[1] LUEDER GERKING[2]

[1] Chemical Engineering, China Textile University, 1882 West Yan-An Road, Shanghai, 200051, People's Republic of China

[2] Karl Fischer Industrieanlagen GmbH, Holzhauser Strasse 157, D-13509 Berlin (Wittenau), Germany

*Received 1 August 1996; accepted 14 October 1997*

**ABSTRACT:** A modified mathematical model based on the melting and recrystallization of an initial distribution of melting temperatures satisfactorily predicts the melting behavior of PET in differential scanning calorimetry. The simulated DSC curves produced in this work agreed fairly well not only with experimental DSC curves performed by Holdsworth et al., but also with the DSC traces provided by SSP PET pellets. The model, taking into account the initial distribution of melting points and the distribution of melting points for the recrystallized material, succeeded in analyzing the origin of dual endotherms of PET with various thermal histories, thereby elucidating the effect of changing crystallization temperature and time, the heating rate in the DSC heating scan, as well as the SSP process on the melting behavior of PET completely. Furthermore, it has been analytically proven that the crystallinity measured on a DSC diagram could not be equal to the weight percentage of crystalline state in the initial specimen. The deviation of the measured crystallinity, as observed relevant to the melting and recrystallization processes, is caused by the changes of the heat of fusion with the melting temperature as well as the difference of heat capacities of liquid and solid-state polymer. © 1998 John Wiley & Sons, Inc. J Appl Polym Sci 69: 729–742, 1998

## INTRODUCTION

Multiple melting endotherms during differential scanning calorimetric measurements have been observed with many polymers, including poly(ethylene terephthalate) (PET),[1–12] poly(butylene terephthalate) (PBT),[13,14] polyethylene (PE),[15,16] polypropylene (PP),[17,18] poly(phenylene sulfide),[19] and the aliphatic nylons,[20,21] for many years. Early works[1–5] assumed that the dual melting endotherms of PET corresponded to melting of two crystalline structures initially present in the sample, such as folded-chain crystallites and bundle crystals, each associated with a different melting temperature. Thus, the two endothermic fusion peaks could be explained in terms of a bimodal distribution of melting temperatures. Other workers[6–8] claimed that crystallites, which formed at low temperatures, present in the sample prior to the DSC scan would undergo a continuous perfection process as a result of partial melting and recrystallization during the scan. This continuous perfection process could lead to an increase in the overall crystallinity.[7] Furthermore, Todoki and Kawaguchi[20] suggested that the pair of melting peaks of nylon 66 fibers in a thermal analysis could arise from an initial single-peak crystal distribution, which was undergoing melting, recrystallization, and remelting during an upward scan in temperature. Their conclusions have since been confirmed analytically by Yagfarov.[22,23] Hence, it is clear that

*Correspondence to:* Z. L. Tang.

Journal of Applied Polymer Science, Vol. 69, 729–742 (1998)
 CCC 0021-8995/98/040729-14

the DSC scans may not represent the genuine state of the material at room temperature before scanning.

More recently, Cebe and Chung[19] pointed out that two different sizes of crystals present in each of two different types of spherulites could lead to more than two endotherms during DSC scanning of PBT, which had been cooled at a constant rate from the melt state. However, Cheng and Wunderlich[24] have suggested that the multiple melting peaks might arise from melting and recrystallization taking place during scanning in the calorimeter and were not indicative of the morphology that was present at room temperature before scanning. Nichols and Robertson[25] have investigated the melting behavior of PBT specimens prepared by cooling the molten polymer from 250 to 30°C at specific constant rates. Meanwhile, they have proposed a model that was based on the simultaneous melting and recrystallization of an initial distribution of crystal melting temperatures that contained only one maximum and two inflection points. Satisfactory agreement between the experimental and simulated curves by using this model indicated that three melting endotherms could arise solely from the melting and recrystallization of a single original population of crystals.

However, in Nichols and Robertson's work[25] the best fits of their simulated curves to the experimental data were obtained by assuming that the material was initially 100% crystalline, although the crystallized specimens undoubtedly contained some amorphous fraction. Another specific question posed was whether the melting and recrystallization have effects on the measurement of crystallinity of the specimen by DSC. Moreover, such effects existing, what could be the mechanism by which they influence the measurement? On the other hand, for preparing PET with molecular weight greater than 20,000 suitable for industrial applications, solid-state polycondensation (SSP) is generally employed. Here, the amorphous PET pellets produced by melt polycondensation undergo isothermal crystallization at 180–190°C, where the maximum crystallization rate occurs, for an appropriate time period. Then SSP is carried out by heating the crystallized polymer pellets at a higher temperature but below the melting temperature, generally at 210–240°C so that the crystallized PET is virtually subjected to an annealing treatment during the SSP. Doubtless, annealing of isothermally crystallized PET would result in structural changes, markedly influencing the melting behavior of the polymer. Therefore it is particularly significant for industry to investigate how the SSP operation conditions affect melting behavior of PET.

On the basis of Nichols's work[25] we propose an improved model based on the melting and recrystallization to predict the melting behavior of PET in a scanning calorimeter. The simulated DSC curves we produced agree fairly well not only with the traditional experimental DSC curves performed by Holdsworth et al.[7] but also with the DSC traces provided by our SSP PET pellets. Herein, the origins of single or dual melting endotherms for specimens with various thermal histories can be explained by the simulation, indicating the effects of changing crystallization temperature and time, the heating rate for DSC scanning, as well as the SSP process, on the melting behavior completely. Meanwhile the model has been used to prove that the crystallinity measured on a DSC diagram could not be equated to the weight percentage of crystalline state in the initial specimen. The deviation of the measured crystallinity, as observed relevant to the melting and recrystallization processes, is caused by the changes of the heat of fusion with the melting temperature as well as the difference of heat capacities of liquid and solid state polymer.

## EXPERIMENTAL

### Material

PET was obtained from KARL FISCHER GmBH Germany, in the form of small pellets with the initial molecular weight above 21,000.

### Specimen Preparation

Specimens were prepared in the DSC under a nitrogen atmosphere with procedure conditions suitable for solid-state polycondensation as shown in Table I.

### Differential Scanning Calorimetry

Thermal analysis of the treated PET pellets with the above conditions was performed using a Metteler Model 12E differential scanning calorimeter. The position and area and the melting peaks on

**Table I Experimental Conditions for PET Samples in the DSC**

| Sample | Mass (mg) | Scanning Rate 50 → 180°C (°C/min) | Isothermal Crystallization at 180°C (min) | Scanning Rate 180 → 220°C (°C/min) | Annealing at 220°C (min) | Scanning Rate 220 → 50°C (°C/min) | DSC Measurement at Scanning Rate (°C/min) |
|---|---|---|---|---|---|---|---|
| 1 | 10.30 | 20 | 20 | 20 (180 → 200°C)<br>0.1 (200 → 220°C) | 0 | −20 | 10 |
| 2 | 16.20 | 20 | 60 | 20 | 60 | −20 | 10 |
| 3 | 10.90 | 20 | 20 | 20 (180 → 200°C)<br>0.2 (200 → 220°C) | 360 | −20 | 10 |
| 4 | 12.60 | 20 | 60 | 20 | 540 | −20 | 10 |

heating were recorded for each run, using control and evaluation software TA 89A.

## DSC SIMULATION

### Mathematical Model

The wide and variable melting range of a polymer is attributable in large measure to variations in lamellar thickness and crystal defect. The differences of crystal sizes and degrees of crystal perfection cause an initial melting distribution, $C_i(T)$, of the sample with experimental thermal histories such as cooling at a constant rate from the melt, cold crystallization from the amorphous state, and then cooling to room temperature or annealing at higher temperature. If the crystallization process takes place over a long time or small temperature interval, or annealing process of the precrystallized polymer proceeds relatively long, the differences of lamellar thickness and crystal defect become small, which yields a narrow initial melting distribution. The following simple function has been used for the initial distribution of melting points of PET sample

$$C_i(T) = N \cdot (T_m^* - T) \cdot (1-p)^2 \cdot p^{(T_m^* - T)} \quad (1)$$

$$N = \frac{1}{\int_{T_{\min}}^{T_m^*} (T_m^* - T) \cdot (1-p)^2 \cdot p^{(T_m^* - T)} dT} \quad (2)$$

where $T_m^*$ is the maximum melting temperature of any crystals originally present in the sample, $p$ is the curve shape factor, $N$ is the normalization constant, and $T_{\min}$ is 100°C, the lowest melting temperature of any crystals originally present in the sample.

With the normalization constant introduced above, the weight fraction of crystals that have melting temperatures between $T \sim T + dT$ to total initial crystals is $C_i(T)dT$.

If the weights of the initial crystals and the total sample are $W_c$ and $W$, the crystallinity of the sample before DSC scan is

$$X_c = \frac{W_c}{W} \quad (3)$$

Therefore, the weight percentage of crystals which have melting temperatures between $T \sim T + dT$ to sample is $X_c \cdot C_i(T)dT$.

The distribution $C_i(T)$ has the same form as that used for the molecular weight distribution resulting from a polycondensation. The width and position of the distribution on the temperature axis can easily be adjusted by changing the values of $p$ and $T_m^*$ to simulate the initial melting temperature distributions of the samples with various thermal histories (see Fig. 1). As $p$ is increased, the distribution becomes broader and the position

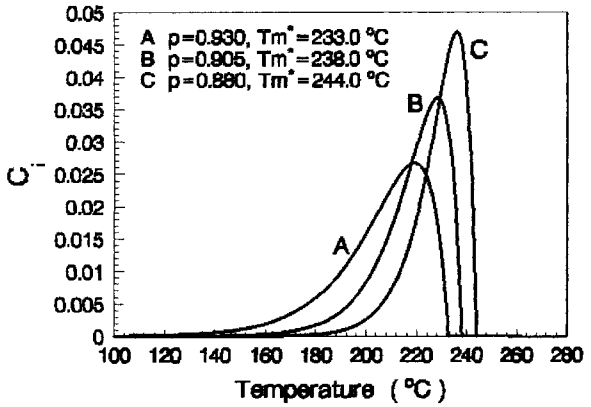


**Figure 1** Representative initial distributions of crystal melting temperatures used to model PET with various crystallization from amorphous.

of the maximum moves slightly to lower temperature side. As $T_m^*$ is increased, the distribution is shifted to higher temperatures. Because the distribution $C_i(T)$ does not go to zero at the low temperature extreme, we assume the lowest melting temperature is 100°C, thereby, $C_i(T \leq 100) = 0$.

If the heating rate for DSC scanning is slow enough, the crystals that have melting temperatures below the present temperature $T(t)$ could be molten. The recrystallization rate, $b(T)$, is assumed to be proportional to the fraction of crystals that are molten, $m(T)$, and represented by the weight fraction of recrystallized crystals to the total initial crystal in unit time

$$b(T) = m(T)G(T) \tag{4}$$

The weight of recrystallized crystals per unit weight of sample in unit time will be expressed as

$$W_r = X_c \cdot m(T)G(T) \tag{5}$$

$G(T)$ is the growth rate of the polymer crystals with the unit of time$^{-1}$, which some previous authors[25] mistook for mass/time, and described by a function of the form

$$G(T) = A \cdot \exp\{-[(T_{\max} - T)/s]^2\} \tag{6}$$

$T_{\max}$ is the temperature of maximum growth rate, $A$ and $s$ are constants that adjust the height and width of the curve. For a given polymer these three parameters are specified constants.

Polymer crystals that melt during heating may recrystallize to crystals with a higher melting temperature, if the recrystallization rate is high enough. The melting temperature of the new crystals is determined by the temperature difference between the theoretical equilibrium melting temperature, $T_m^0$, and the temperature at which the new crystals form, $T_c$. The new melting point can be expressed as[26]

$$T_m = k(T_m^0 - T_c) + T_c \tag{7}$$

The coefficient, $k$, is a fraction between zero and one.

To rearrange eq. (7) gives

$$T_c = \frac{T_m - kT_m^0}{1 - k} \tag{8}$$

While the temperature increase from $T_c$ to $T_c + dT_c$ in the time interval $dt$ at a heating rate, $q = dT_c/dt$, the melting points of the new crystals, which recrystallized over this time interval, distribute in the temperature range of $T_m \sim T_m + dT_m$. The derivative of eq. (7) is

$$\frac{dT_c}{dT_m} = \frac{1}{1 - k} \tag{9}$$

Then, we represent the melting point distribution for the recrystallized material by $R_i(T)$. Therefore, $R_i(T_m)dT_m$ is the weight fraction of the new crystals that have melting temperatures between $T_m \sim T_m + dT_m$. From eq. (4) we obtain

$$R_i(T_m)dT_m = b(T_c)dt = m(T_c)G(T_c)dt \tag{10}$$

Substituting $q = dT_c/dt$, eqs. (8) and (9) into eq. (10) and arranging it leads to

$$R_i(T) = \frac{m\left(\frac{T - kT_m^0}{1 - k}\right) \cdot G\left(\frac{T - kT_m^0}{1 - k}\right)}{(1 - k) \cdot q} \tag{11}$$

During a heating scan in a DSC, the cumulative amount of crystals that has melted at and below the temperature $T$ is denoted by $M_i(T)$, which consists of two parts: the cumulative fraction of crystals in the initial distribution that has melted, and the cumulative fraction of crystals with melting points below $T$ in the distribution of recrystallization material, representing the part of the recrystallized material that has melted again. Thus,

$$M_i(T) = \int_{T_s}^{T} [C_i(T) + R_i(T)]dT \tag{12}$$

The fraction of crystals that is molten at any temperature during an upward scan in temperature is the difference between $M_i(T)$ and the total weight fraction of crystals that has recrystallized during the heating process from start temperature, $T_s$, to $T$, i.e.,

$$m(T) = M_i(T) - \int_0^{t(T)} m[T(t')]G[T(t')]dt' \tag{13}$$

Thence, the weight of the molten crystals per unit weight of sample at this temperature is

$$M(T) = X_c \cdot m(T) \tag{14}$$

The derivative of $m(T)$ with respective to temperature expresses the rate of increase of the molten crystals fraction:

$$\frac{dm(T)}{dT} = C_i(T) + R_i(T) - m[T(t)]G[T(t)]\frac{dt}{dT} \tag{15}$$

Because the lowest melting temperature of the recrystallized material is $T_b = k(T_m^0 - 100) + 100$, eq. (15) can be represented as

$$\frac{dm(T)}{dT} = \begin{cases} C_i(T) - m[T(t)]G[T(t)]/q & T < T_b \quad \text{(16-a)} \\ C_i(T) + R_i(T) - m[T(t)]G[T(t)]/q & T \geq T_b \quad \text{(16-b)} \end{cases}$$

Apparently, eq. (16-a, b) looks like a first-order nonhomogeneous differential equation with the standard form $m'(T) + P(T)m(T) = Q(T)$, given $P(T)$ and $Q(T)$ are known functions of $T$, which some authors[25] integrated to reach an analytical solution as

$$m(T) = \left\{ C + \int_{T_s}^{T} [C_i(T') + R_i(T')] \times \exp\left( \int_{T_s}^{T'} \frac{G(T'')}{q} dT'' \right) dT' \right\} \times \exp\left[ -\int_{T_s}^{T} \frac{G(T')}{q} dT' \right] \tag{17}$$

However, this approach lacks mathematical clarity for the reason that the first integral involving $R_i(T')$, which as shown by eq. (11) is not a given function but one associated with the function looked for in the form of $m[(T - kT_m^0)/(1 - k)]$ with a shifter of variable $T$.

During an experiment in a DSC, the power input to the sample to maintain a constant heating rate is monitored as a function of temperature. The DSC signal depends on the sample average heat capacity, plus any additional heat absorbed or evolved during phase changes, such as the power required to melt any crystals at their melting temperature and the power released by the specimen during recrystallization.

While the temperature increases from $T$ to $T + dT$ in the time interval $dt$ at a constant heating rate, $q = dT/dt$, the weight change of the molten crystals, $dM$, occurs, and the heat input per unit mass of sample in the DSC is

$$dQ = \Delta H_f \cdot dM + C_{pl}[M + (1 - X_c)]\, dT + C_{ps}(X_c - M)\, dT \tag{18}$$

$\Delta H_f$ is the heat of fusion of polymer crystal, with unit of J $g^{-1}$, $C_{pl}$ is the heat capacity of liquid polymer, with unit of J $g^{-1}$ $K^{-1}$, and $C_{ps}$ is the heat capacity of polymer crystal, with unit of J $g^{-1}$ $K^{-1}$. Substituting eq. (14) and $\Delta C_p^*$ for the heat capacity difference $C_{pl} - C_{ps}$, the input heat $dQ$ becomes

$$\begin{aligned} dQ &= \Delta H_f \cdot X_c\, dm + \Delta C_p^* X_c m(T)\, dT + (C_{pl} - \Delta C_p^* X_c)\, dT \\ &= dH_f + dQ_1 + dQ_2 \end{aligned} \tag{19}$$

The heat change per unit temperature rise, in terms of heat capacities, will be

$$\begin{aligned} C_p = \frac{dQ}{dT} &= \Delta H_f \cdot X_c \frac{dm}{dT} + \Delta C_p^* X_c m(T) + (C_{pl} - \Delta C_p^* X_c) \\ &= \frac{dH_f}{dT} + \frac{dQ_1}{dT} + \frac{dQ_2}{dT} \end{aligned} \tag{20}$$

Seeing the linear relationships of $C_{pl}$ and $C_{ps}$ vs. temperature $T$,[27] the last term of eq. (20), $dQ_2/dT$, is responsible for the baseline. The first term $dH_f/dT$ responsible for latent heat, and the second term $dQ_1/dT$ due to the difference of heat capacities, both contribute to melting peaks.

Generally, in a DSC experiment diagram, the area of the melting peak with reference to the heat capacity baseline is considered as the experimental heat of fusion per unit mass of sample, $\Delta H_{\text{exp}}$, usable for weight fraction crystallinity determination as shown in eq. (21)[24]:

$$X_c^{\text{dsc}} = \frac{\Delta H_{\text{exp}}}{\Delta H_f^0} \tag{21}$$

where $\Delta H_f^0$ is the heat of fusion of 100% perfect crystal with unit of J $g^{-1}$. Chen et al.[28] have

shown that the widely used crystallinity obtained by eq. (21) can be called the "equivalent weight crystallinity," signifying the amount of perfect crystals that can melted by the measured enthalpy of melting. The equivalent weight crystallinity does not only depend on the amount of the crystals, but also on the perfection of the crystals: A crystal with higher perfection has a larger equivalent weight.

There are usually three characteristic temperatures that are considered as essential for melting peaks: the onset temperature, i.e., the lowest melting temperature of any crystals originally present in the sample $T_{\min}$, the peak (maximum) temperature, and the melting-end temperature, $T_{\text{end}}$, up to which all of the crystals have been melted. Substituting the integral of the first two terms of eq. (19) into eq. (21) gives

$$X_c^{\text{dsc}} = \frac{\int_{T_{\min}}^{T_{\text{end}}} (dH_f + dQ_1)}{\Delta H_f^0} = X_c \int_{T_{\min}}^{T_{\text{end}}} \frac{\Delta H_f}{\Delta H_f^0}\, dm + \frac{X_c}{\Delta H_f^0} \int_{T_{\min}}^{T_{\text{end}}} \Delta C_p^* m(T)\, dT = X_c^0 + \Delta X_c \qquad (22)$$

### Simulation

Using the Runge-Kutta method to seek a numerical solution of eq. (16-a, b) incorporating eqs. (11) and (22), we are in a position to simulate the melting behavior of a sample in a scanning calorimeter via eq. (20).

For the specific example of PET, $\Delta H_f^0 = 140$ J $g^{-1}$, the heat capacity as a function of temperature is known for the liquid, and the solid-state heat capacity was estimated by assuming the same temperature dependence but shifted down by 0.406 J $g^{-1}$ $k^{-1}$, which is the $\Delta C_p^*$ at the glass transition temperature for PET.[25,27]

Furthermore, the changes in heat of fusion with the melting temperature were introduced for these simulations. Based on the assumptions underlying the well known Thomas–Gibbs equation, the heat of fusion of chain-folded crystals at melting temperature $T_m$ was given by[28]

$$\Delta H_f = \Delta H_f^0 \frac{T_m}{T_m^0} \qquad (23)$$

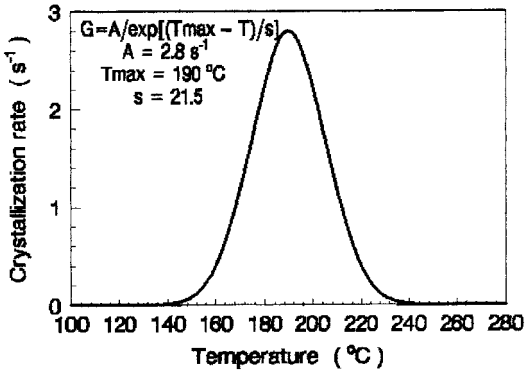


**Figure 2** Crystallization rate behavior used to simulate DSC curves of PET.

Obviously, the better the perfection of crystal, the higher the melting temperature and the larger the heat of fusion. It indicates that the crystallinity obtained by eq. (22) is dependent on the perfection of the crystals.

Cobbs[29] reported the overall crystallization rate of PET was fastest at temperatures from 180 to 190°C. Yoon[30] measured the density crystallinities of PET samples that isothermally crystallized at various temperature, and found the crystallization rate was fastest at 190°C. According to this, a value of $T_{\max} = 190$°C has been used for simulating the DSC curves. The values of $A$ and $s$ in eq. (6), $k$ in eq. (7), and $p$ and $T_m^*$ in eq. (1) were coordinately adjusted for the simulation to obtain the best fits to experimental data. The same growth rate of crystallization $G(T)$ was used for all the simulated curves and is shown in Figure 2. To model the experimental curves of samples with various thermal histories for each sample, a distinctive initial distribution of melting points was assumed by changing the values of $p$ and $T_m^*$ in eq. (1). The values of these parameters for simulation are shown in Table II.

## EXPERIMENTAL RESULTS

### Traditional Experimental Results of Holdsworth et al.[7]

Samples of amorphous PET film were heat crystallized by heating in a Perkin–Elmer DSC-1 calorimeter from room temperature to the required temperature, holding at this temperature for a given time, and then cooling to room temperature.

**Table II Parameters Determined by Simulating Various Experimental DSC Curves**

| | Figure 3(b) | | | | | | | Figure 5(b) | | | | Figure 7(b) | | | | Figure 9(b) | | | |
|---|---|---|---|---|---|---|---|---|---|---|---|---|---|---|---|---|---|---|---|
| | B | C | D | E | F | G | | A | B | C | D | A | B | C | D | 1 | 2 | 3 | 4 |
| $A$ ($s^{-1}$) | | | | | | | | 2.8 | | | | | | | | | | | |
| $T_{max}$ (°C) | | | | | | | | 190 | | | | | | | | | | | |
| $s$ | | | | | | | | 21.5 | | | | | | | | | | | |
| $k$ | 0.56 | 0.50 | 0.28 | 0.26 | 0.24 | 0.30 | | 0.60 | 0.54 | 0.50 | 0.10 | 0.20 | 0.36 | 0.40 | 0.42 | 0.55 | 0.53 | 0.30 | 0.15 |
| $T^{\circ}_m$ (°C) | | | | | | | | 280 | | | | | | | | | | | |
| $p$ | 0.92 | 0.91 | 0.764 | 0.758 | 0.75 | 0.86 | | 0.93 | 0.905 | 0.88 | 0.60 | | 0.875 | | | 0.90 | 0.87 | 0.86 | 0.78 |
| $T^{*}_m$ (°C) | 236.1 | 249.4 | 257.7 | 259.4 | 260.9 | 261.7 | | 233.0 | 238.3 | 244.0 | 254.1 | | 252.1 | | | 242.0 | 249.8 | 250.5 | 255.3 |
| $q$ (°C/min) | | | 16 | | | | | | 16 | | | 16 | 8 | 4 | 2 | | | 10 | |

In all cases heating and cooling rates of 16°C/min were used. The melting behavior of the samples was examined on the DSC using 10 mg of sample at a scanning rate of 16°C/min, see Figures 3(a) and 5(a) (copy from ref. 7), or at various scanning rates, see Figure 7(a) (copy from ref. 7).

### Experimental Results of SSP Pellets

The melting behaviors on DSC of PET pellets prepared with various procedure conditions practically suitable for SSP as shown in Table I, were recorded at a scanning rate of 10°C/min [see Fig. 9(a)].

## DISCUSSION

The general trends that exist in the experimental data are faithfully reproduced in the simulation, as shown in Figures 3, 5, 7, and 9. The initial distribution of melting points, $C_i(T)$, and the melting point distribution for the recrystallized material, $R_i(T)$, for each experimental curve are plotted in Figures 4, 6, 8, and 10. The information obtained from the regular variation of the position and the shape of $C_i(T)$ and $R_i(T)$ is most useful in analyzing the origin of dual endotherms of PET.

### Influence of Crystallization Temperature on Dual Melting Endotherms

For the specimens prepared by heating to a lower temperature and cooling immediately [curves B and C in Fig. 3(a)], the best fits require a lower value of $T^{*}_m$ and a larger value of $p$, representative of a broader distribution in range of lower temperatures (B and C of Fig. 4), reflecting the smaller, relatively poorer quality crystals present in the samples before scanning. This argument, consistent with other investigators, is that the lower crystallization temperatures lead to relatively thin crystals causing relatively lower melting points.[26,31] As the samples B and C are heated during scanning in a DSC, most parts of the crystals melt in the temperature range of 180–240°C, in which fast crystallization rates occur and many crystals with higher melting temperatures can form by recrystallization. Thus, dual endotherms emerge in the DSC diagram. The shape and height of the first peak at low temperatures is

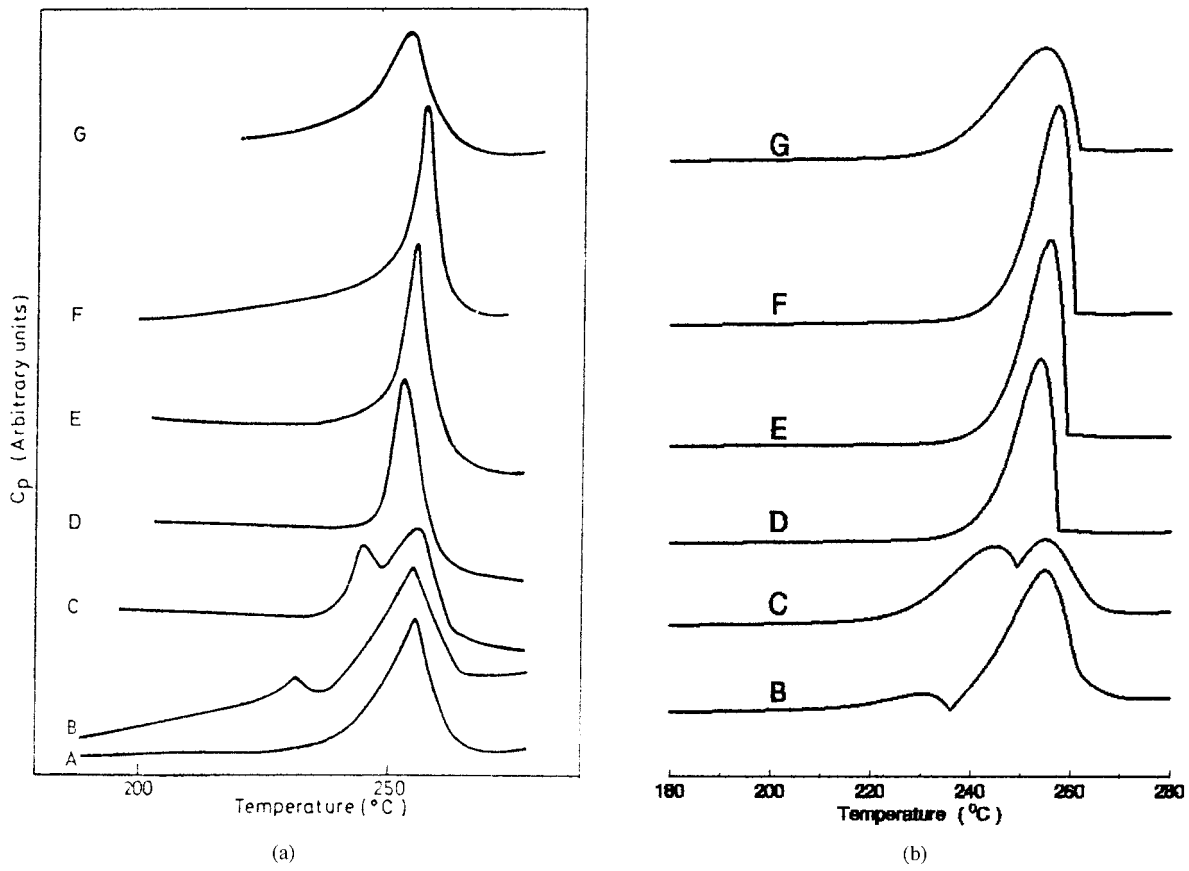


**Figure 3** (a)[7] DSC traces of originally amorphous PET that had been heated to the following temperature (and cooled immediately) (A) amorphous, (B) 224°C, (C) 236°C, (D) 244.5°C, (E) 248.5°C, (F) 252°C, (G) 280°C. (b) The simulated DSC curves associated with Figure 3(a).

determined together by the melting of crystals with little thickness and poor quality that exist in the initial distribution, and the recrystallizing of the molten materials. The second peak at higher temperatures is due to the melting of the more perfect and bigger crystals that are newly recrystallized and had higher melting points other than that of the original material. Also, in B and C, because the initial distribution, $C_i(T)$, and melting point distribution for recrystallized material, $R_i(T)$, are separated rather far apart, the two melting endotherms appear distinguishable.

As a contrast, for the samples prepared by heating to higher temperature and cooling immediately [samples D, E, and F in Fig. 3(a)], the crystals present in the sample become more perfect and consist of thicker lamellae; therefore, the initial distributions become narrower and shift upward in temperature. Only a few crystals melt below 240°C and accordingly, little material is available for recrystallization at temperatures where fast crystallization rate occurs. D, E, and F in Figure 4 show that the melting point distribution of recrystallized crystals, $R_i(T)$, has a much smaller area than the initial distribution, $C_i(T)$, and furthermore, $C_i(T)$ and $R_i(T)$ overlap each other. Consequently, the shape of the simulated DSC curve is essentially similar to the initial distribution of melting points. Moreover, in comparison with samples D, E, and F, the broader DSC trace of sample G, that was prepared by heating to 280°C, at which the polymer was completely melted, and cooling immediately from the molten state is due to a somewhat broader initial distribution in the higher temperature range, because the specimen was crystallized through a wider and higher temperature range.

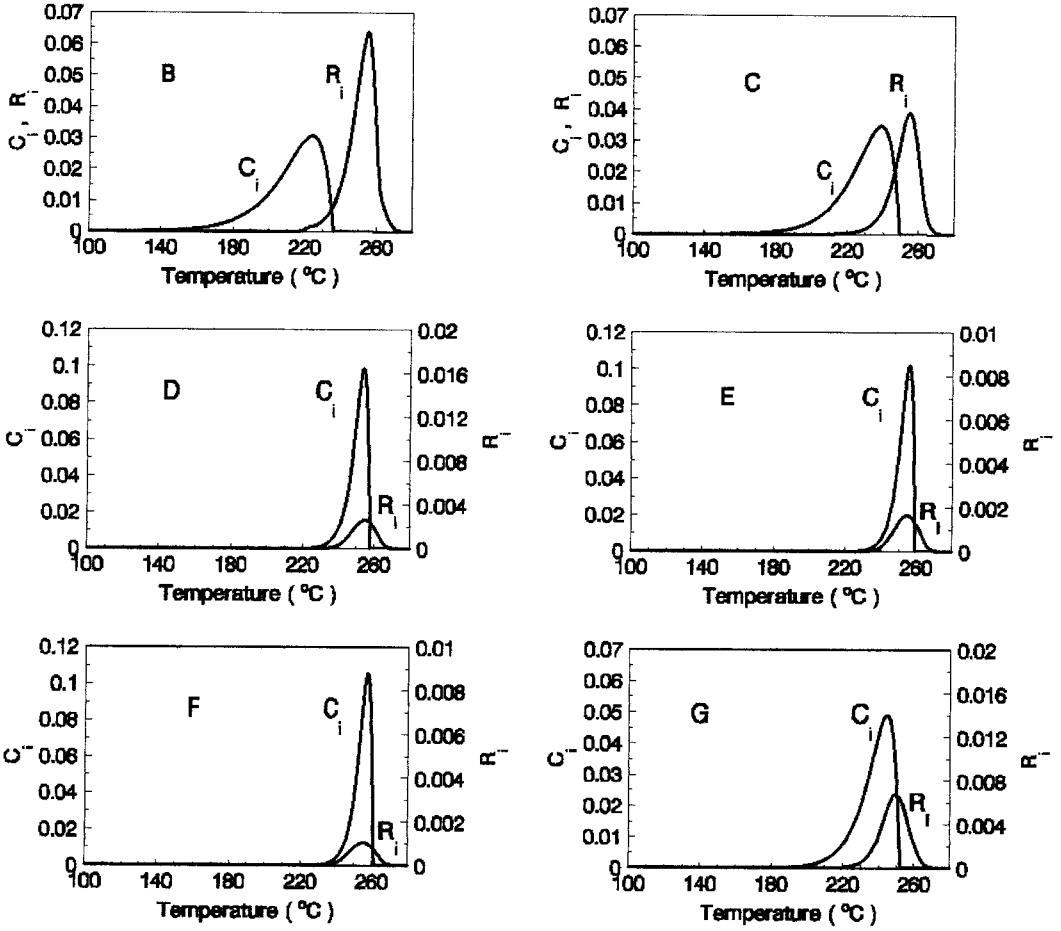


**Figure 4** The initial distributions of crystal melting temperatures $C_i$ and the melting temperatures distributions for the recrystallized materials $R_i$ associated with the simulated DSC curves in Figure 3(b).

### Influence of Crystallization Time on Dual Melting Endotherms

It is well known that the lamellar thickening and the improving of crystal perfection is controlled by crystallization temperature and time.[26,32] Figure 5(a) shows the DSC traces of sample that were heated to 220°C and crystallized for various times and then cooled to room temperature. In the case of heating a sample to 220°C followed by cooling it to room temperature immediately (A in Fig. 5), the poor and thin crystals formed below 220°C have a broader initial distribution in low temperature range. When heated during a DSC scanning upward to 240°C, most parts of the crystals of this sample melt, and many molten crystals can recrystallize simultaneously, causing a little endotherm at low temperatures, thereafter the large endotherm occurs due to the melting of the more perfect and thicker crystals formed by recrystallization. In the case of heating the sample to 220°C and maintaining it at that temperature over a relatively short time (B and C in Fig. 5), the poor crystals formed at lower temperatures will improve in perfection and increase the thickness of lamellae only to a limited degree, so that the initial distribution in the higher temperature range appears narrower. When both samples are heated in DSC scanning, most parts of the initial crystals melt above 220°C, where only slow crystallization rates exist, it happens that the narrower and in the higher temperature range the initial distribution is, the higher the melting and recrystallizing temperatures are and the less new crystals form by recrystallization. Therefore, the low temperature endotherm associated with melting of initial distribution and recrystallizing of molten material becomes larger and moves closer to high tem-

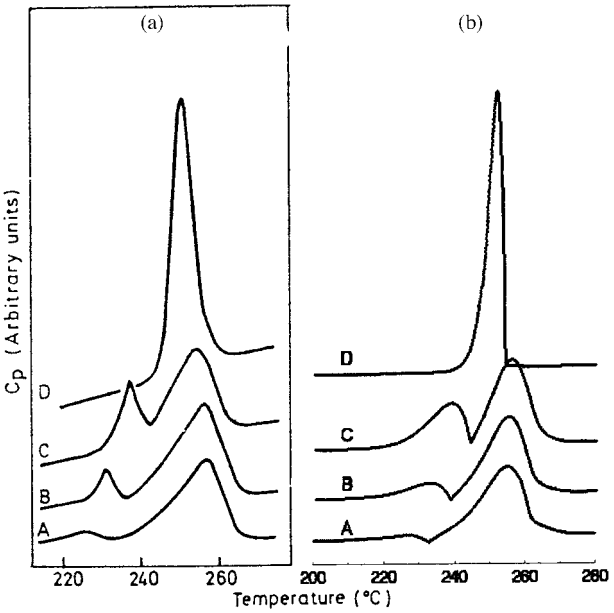


**Figure 5** (a)[7] DSC traces of PET samples crystallized at 220°C for: (A) 0 min, (B) 5 min, (C) 30 min, (D) 960 min. (b) The simulated DSC curves associated with Figure 5(a).

perature endotherm with the increase of the crystallization time at 220°C. Only when the crystallization time at temperature 220°C lasted a long time, such as several hundreds minutes, the perfection processes of crystallization and thickening of lamellae may have enough time to cause the initial distribution, which becomes a very sharp peak, centered at a sufficiently high temperature. At this temperature range crystallization rate is nearly zero, corresponding to an extremely small $R_i(T)$ (Fig. 6). Consequently only a high single endothermic peak occurs.

### Influence of Scanning Rate in DSC on Dual Melting Endotherms

As shown in Figure 7, the scanning rate in a DSC influences dramatically the shape and height of the two endotherms. At a fast upward scanning rate of temperature, only one melting peak is evident. But as the rate is reduced, a second peak appears, and the lower the rate, the higher the temperature and the larger the size of the second peak will be. This effect is explicable on the basis of our foregoing model as a result of the inverse dependence of $R_i(T)$ on scanning rate $q$ in eq. (11). When the scanning rate decreases, $R_i(T)$ and $k$ in eq. (7) increase because of all the processes of recrystallization, perfection of the crystals and thickening of the lamellae have more time to proceed throughout the scanning. Accordingly, the melting point distribution of recrystal-

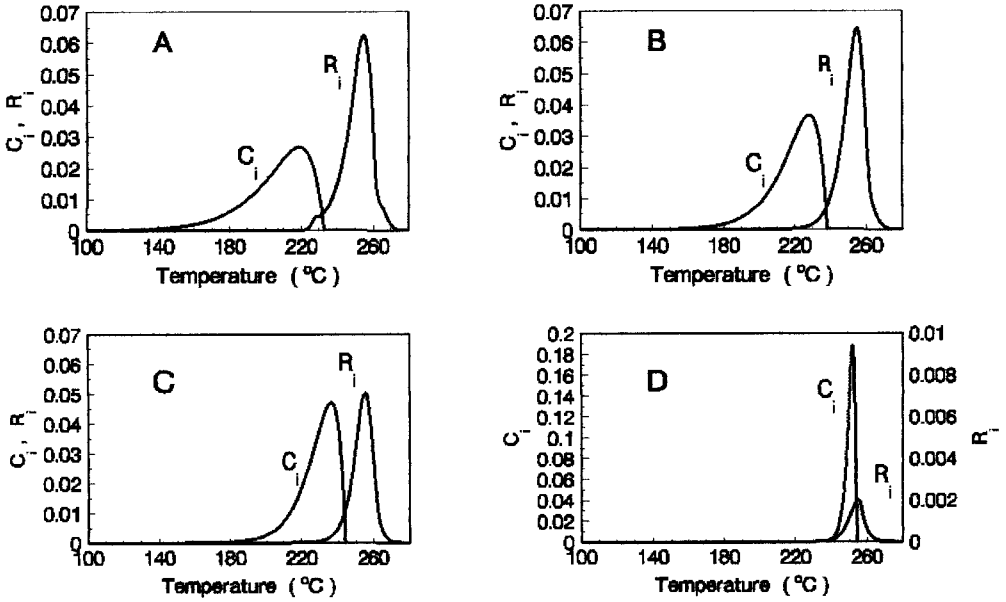


**Figure 6** The initial distributions of crystal melting temperatures $C_i$ and the melting temperatures distributions for the recrystallized materials $R_i$ associated with the simulated DSC curves in Figure 5(b).

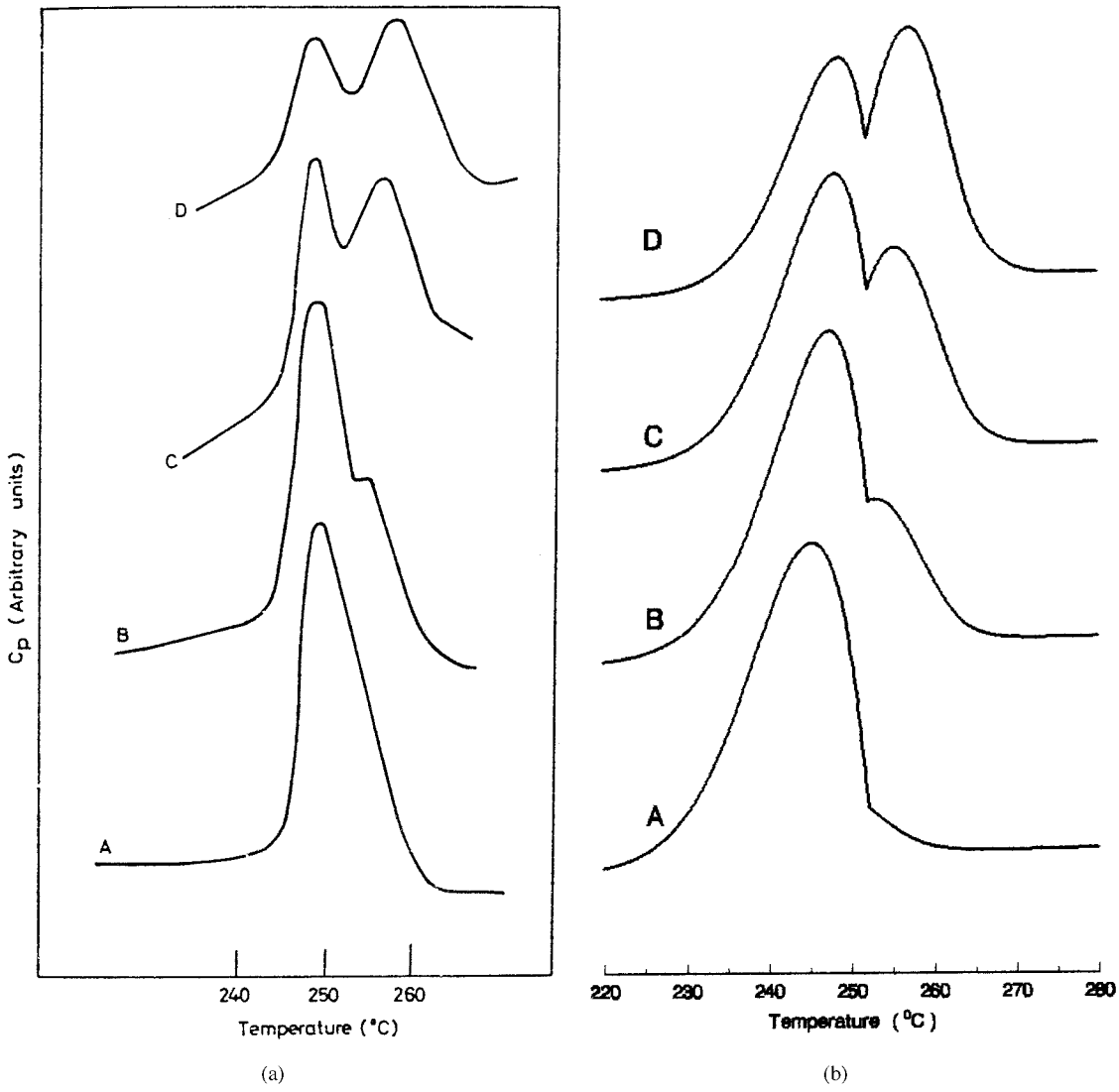


**Figure 7** (a)[7] DSC traces of PET that had been crystallized at 240°C for 5 min and recorded at heating rates of (A) 16°C/min, (B) 8°C/min, (C) 4°C/min, (D) 2°C/min. (b) The simulated DSC curves associated with Figure 7(a).

lized material increases in size with the peak moving slightly to a high temperature. The calculated $R_i(T)$ shifting to a higher temperature and increasing in size with decreases of scanning rate can be seen in Figure 8.

### Influence of SSP Treatment on Dual Melting Endotherms

Despite the fact that sample 1 is crystallized isothermally at a lower temperature, it still has a first endotherm lying in a range of a relatively higher temperature, compared with sample A in Figure 5. This is because of the slow heating rate that follows isothermal crystallization, improving the perfection of the isothermally formed crystal. Under similar crystallization conditions as sample 1, the first endotherm of sample 3 shifts to a high temperature with a narrower and higher shape. This implies SSP results in a better perfection of the crystals formed during the procedure before SSP. Compared with sample 2, sample 4 has a narrower and higher $C_i$ lying in a range of a higher temperature with a much smaller $R_i$, causing both endothermic peaks in DSC to merge. This con-

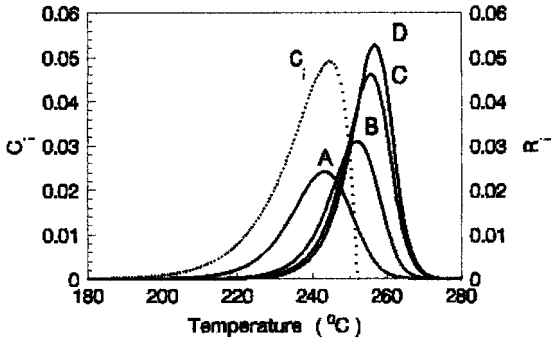


**Figure 8** The initial distributions of crystal melting temperatures $C_i$ and the melting temperatures distributions for the recrystallized materials $R_i$ associated with the simulated DSC curves in Figure 7(b).

cludes that the longer the SSP proceeds, the more perfect the crystal performs, in addition to the increase of molecular weight of the polymer.

### Crystallinity Measured on DSC

The crystal begins to melt at temperature $T_{\min}$, at which $m(T_{\min}) = 0$. Correlating with eq. (23), the first term of eq. (22) gives rise to

$$X_c^0 = \frac{X_c \cdot \int_{T_{\min}}^{T_{\text{end}}} \Delta H_f \, dm}{\Delta H_f^0} = \frac{X_c}{T_m^0} \cdot \int_{T_{\min}}^{T_{\text{end}}} T \, dm$$

$$= \frac{X_c}{T_m^0} \left[ T_{\text{end}} m(T_{\text{end}}) - \int_{T_{\min}}^{T_{\text{end}}} m(T) \, dT \right] \quad (24)$$

Integrating eq. (10), one obtains the total weight of the recrystallized material

$$CR = X_c \cdot \int_{T_{\min}}^{T_{\text{end}}} R_i(T) \, dT$$

$$= X_c \cdot \int_{t(T_{\min})}^{t(T_{\text{end}})} m[T(t')] G[T(t')] \, dt' \quad (25)$$

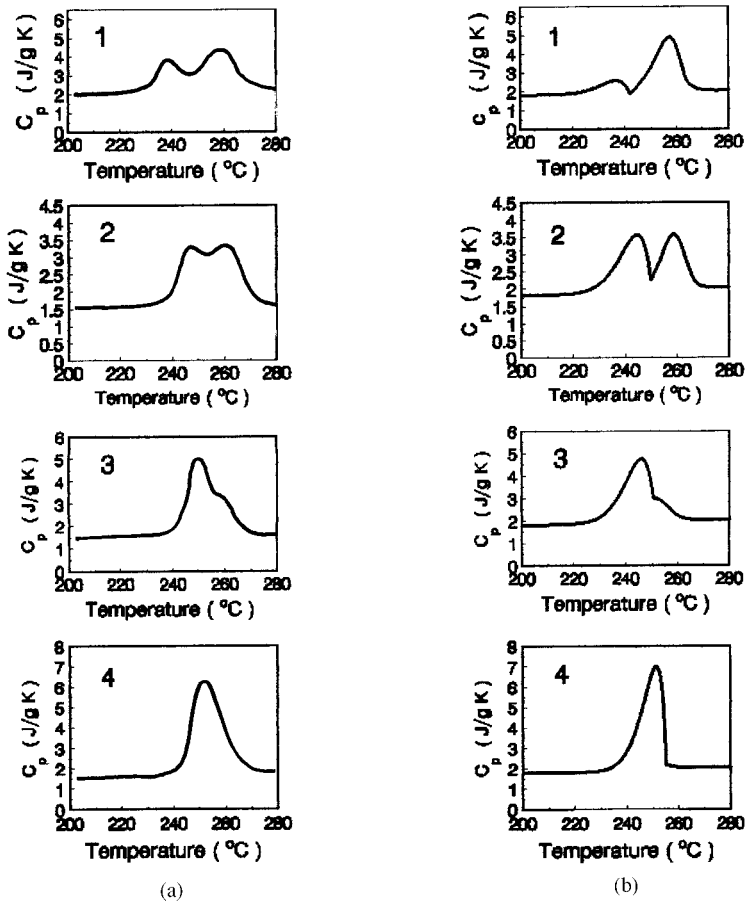


**Figure 9** (a) DSC traces of PET prepared with procedure conditions practically suitable for SSP as shown in Table I and recorded at heating rates of 10°C/min. (b) The simulated DSC curves associated with Figure 9(a).

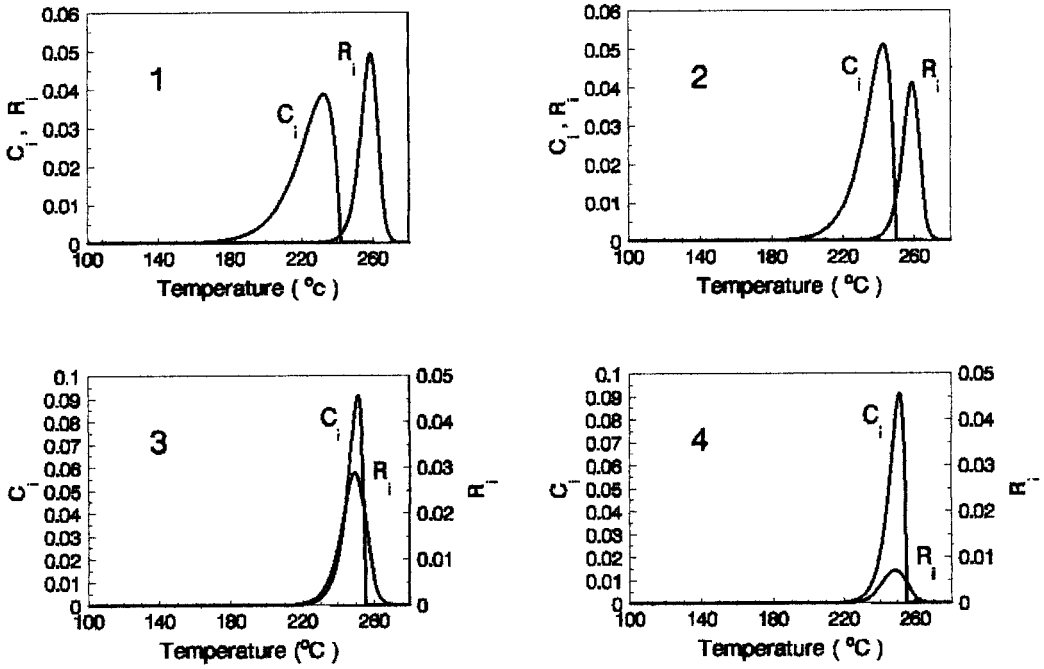


**Figure 10** The initial distributions of crystal melting temperatures $C_i$ and the melting temperatures distributions for the recrystallized materials $R_i$ associated with the simulated DSC curves in Figure 9(b).

Integrating eq. (15) with incorporating eq. (25) and normalization condition gives

$$m(T_{\text{end}}) = \int_{T_{\min}}^{T_{\text{end}}} C_i(T)\,dT + \int_{T_{\min}}^{T_{\text{end}}} R_i(T)\,dT - \int_{t(T_{\min})}^{t(T_{\text{end}})} m[T(t')]G[T(t')]\,dt' = \int_{T_{\min}}^{T_{\text{end}}} C_i(T)\,dT = 1 \quad (26)$$

Substituting eq. (26) into (24) then

$$X_c^0 = X_c \frac{T_{\text{end}}}{T_m^0} - \frac{X_c}{T_m^0} \int_{T_{\min}}^{T_{\text{end}}} m(T)\,dT \quad (27)$$

Eventually, the measured crystallinity in DSC is

$$X_c^{\text{dsc}} = X_c^0 + \Delta X_c = X_c \frac{T_{\text{end}}}{T_m^0} + X_c \left[ \frac{1}{\Delta H_f^0} \int_{T_{\min}}^{T_{\text{end}}} \Delta C_p^* m(T)\,dT - \frac{1}{T_m^0} \int_{T_{\min}}^{T_{\text{end}}} m(T)\,dT \right] \quad (28)$$

Equation (28) provides a noteworthy conclusion that the measured crystallinity from a DSC scan curve, $X_c^{\text{dsc}}$, should be equal to initial crystallinity of the sample multiplied by the melting point ratio $T_{\text{end}}/T_m^0$, plus a second term. The second term is due to the difference of heat capacities between liquid and solid polymer, and the difference of heats of fusion between the 100% perfect crystal and the unperfect one. Besides, it is also associated with $m(T)$, the fraction of molten crystals at any temperature that is determined by the melting and recrystallizing processes. Conceivably, when the melting points of the initial crystals distribute uniformly around $T_m^0$, i.e., $\Delta H_f = \Delta H_f^0$, and $\Delta C_p^*$ is negligibly small, the measured crystallinity from eq. (22) could represent the weight percentage of the initial crystals in a sample subject to DSC scan.

The authors are grateful to the National United Chemical Engineering Laboratory, China, East China University of Science and Technology for its financial support.

## REFERENCES

1. R. C. Roberts, *Polymer,* **10,** 113 (1969).
2. R. C. Roberts, *Polymer,* **10,** 117 (1969).

3. J. P. Bell and J. H. Dumbleton, *J. Polym. Sci., A-2,* **7,** 1033 (1969).
4. J. P. Bell and T. J. Murayama, *J. Polym. Sci., A-2,* **7,** 1059 (1969).
5. R. C. Roberts, *J. Polym. Sci., B,* **8,** 381 (1970).
6. D. L. Nealy, T. G. Davis, and C. J. Kibler, *J. Polym. Sci., A-2,* **8,** 2141 (1970).
7. P. J. Holdsworth and T. A. Jones, *Polymer,* **12,** 195 (1971).
8. G. E. Sweet and J. P. Bell, *J. Polym. Sci., A-2,* **10,** 1273 (1972).
9. H. J. Berndt and A. Bossman, *Polymer,* **17,** 241 (1976).
10. S. Fakirov, E. W. Fischer, R. Hoffmann, and G. F. Schmidt, *Polymer,* **18,** 1121 (1977).
11. G. C. Alfonso, E. Pedemonte, and L. Ponzetti, *Polymer,* **20,** 104 (1979).
12. H. J. Oswald, E. A. Turi, P. J. Harget, and Y. P. Khanna, *J. Macromol. Sci. (Phys.),* **3,** 231 (1977).
13. H. J. Ludwig and P. Eyerer, *Polym. Eng. Sci.,* **28,** 143 (1988).
14. J. T. Yeh and J. Runt, *J. Polym. Sci., Polym. Phys. Ed.,* **27,** 1543 (1989).
15. R. B. Prime and L. Melillo, *J. Polym. Sci., A-2,* **7,** 2091 (1969).
16. I. R. Harrison, *J. Polym. Sci., A-2,* **11,** 991 (1973).
17. K. D. Pae and J. A. Sauer, *J. Appl. Polym. Sci.,* **12,** 1921 (1968).
18. R. J. Samuels, *J. Polym. Sci., A-2,* **13,** 1417 (1975).
19. P. Cebe and S. Chung, *Polym. Compos.,* **11,** 265 (1990).
20. M. Todoki and T. Kawaguchi, *J. Polym. Sci., Polym. Phys. Ed.,* **15,** 1067 (1977).
21. A. Xenopulos and B. Wunderlich, *J. Polym. Sci., Polym. Phys. Ed.,* **28,** 2271 (1990).
22. M. Sh. Yagfarov, *Polym. Sci., USSR,* **21,** 975 (1980).
23. M. Sh. Yagfarov, *Polym. Sci., USSR,* **24,** 2915 (1982).
24. S. Z. Cheng, R. Pan, and B. Wunderlich, *Makromol. Chem.,* **189,** 2443 (1988).
25. M. E. Nichols and R. E. Robertson, *J. Polym. Sci., Polym. Phys. Ed.,* **30,** 755 (1992).
26. D. C. Bassett, *Principles of Polymer Morphology,* Cambridge University Press, Cambridge, 1981.
27. S. Z. Cheng, R. Pan, H. S. Bu, and M. Y. Cao, *Makromol. Chem.,* **189,** 1579 (1988).
28. H. L. Chen and J. C. Hwang, *Polymer,* **36,** 4355 (1995).
29. W. H. Cobbs and R. L. Burton, *J. Polym. Sci.,* **10,** 275 (1953).
30. K. H. Yoon, M. H. Kwon, M. H. Jeon, and O. O. Park, *Polym. J.,* **25,** 219 (1993).
31. J. D. Hoffman, G. T. Davis, and J. I. Lauritzen, in *Treatise on Solid State Chemistry,* vol. 3, Plenum Press, New York, 1976.
32. M. Imai, K. Kaji, and T. Kanaya, *Macromolecules,* **27,** 24 (1994).